Int. J. Heat Mass Transfer. Vol. 22, pp. 349–360
© Pergamon Press Ltd. 1979. Printed in Great Britain
0017-9310/79/0301-0349 $02.00/0

LOCAL HEAT TRANSFER AND FLUID FLOW CHARACTERISTICS FOR AIRFLOW OBLIQUE OR NORMAL TO A SQUARE PLATE

K. K. TIEN and E. M. SPARROW
Department of Mechanical Engineering, University of Minnesota, Minneapolis, MN 55455, U.S.A.

(*Received* 14 *June* 1978 *and in revised form* 14 *August* 1978)

Abstract—Wind tunnel experiments have been performed to determine the local and average heat-transfer coefficients and the patterns of fluid flow for a square plate situated at various orientations to the flow direction. The naphthalene sublimation technique was employed for the transfer coefficient determinations while the flow patterns adjacent to the plate were made visible by the oil/lampblack technique. The plate orientations used for the average coefficient measurements extended the range previously studied, and the results of these measurements affirmed the insensitivity of the average coefficient to orientation. The local heat- (or mass-) transfer coefficients are presented as contour diagrams in which lines depicting constant values of the coefficient are plotted. In general, the highest heat-transfer coefficients occur near the edges of the plate. These high coefficients are closely coupled to edge-related hydrodynamic phenomena, which include not only the conventional leading edge boundary layer but other processes related to the finite size of the plate. Of particular interest is the fact that for a plate oriented normal to the flow, the lowest coefficients occur in a centrally positioned stagnation region and the coefficients increase from the center of the plate toward the edges. The fluid flow patterns are presented via photographs. The flow is shown to be highly complex and three dimensional. One of the interesting findings is that the stagnation region migrates from a central position at normal incidence to a more forward position as the plate is inclined.

NOMENCLATURE

- A, face area of naphthalene plate;
- c_p, specific heat at constant pressure;
- h, local heat-transfer coefficient;
- $\bar{h}$, average heat-transfer coefficient;
- j, j-factor, equations (2) and (3);
- K, local mass-transfer coefficient;
- $\bar{K}$, average mass-transfer coefficient;
- $\dot{M}$, average rate of mass transfer;
- Pr, Prandtl number;
- Re, Reynolds number, $U_\infty S/\nu$;
- S, side of square plate;
- Sc, Schmidt number;
- St, Stanton number;
- U_∞, free stream velocity.

Greek symbols

- α,ϕ, angles of attack and yaw, Fig. 1;
- α',ϕ', angles of pitch and yaw, Fig. 2;
- ρ, density;
- ν, kinematic viscosity;
- ρ_{nw}, naphthalene vapor concentration at plate surface;
- $\rho_{n\infty}$, naphthalene vapor concentration in free stream.

INTRODUCTION

FORCED convection heat transfer to airflow over an arbitrarily oriented plate represents both a three-dimensional boundary-layer research problem and a prototype situation for numerous applications. The applications include many of contemporary interest such as wind-related heat losses from solar collector plates and from walls and roofs of buildings. For these applications, the quantity that is of most direct relevance is the average heat-transfer coefficient. Information on average heat-transfer coefficients for airflow over square plates was determined experimentally in [1]. It was found there that the transfer coefficients were quite insensitive to the orientation of the plate relative to the airstream. Furthermore, it was demonstrated that the transfer coefficients that have been conventionally employed for the calculation of wind-related heat losses from flat plate solar collectors are seriously in error.

The present study was undertaken as a many-faceted extension of [1], with emphasis placed on the details of the heat transfer and fluid flow distributions and with lesser weight placed on the average coefficients. To this end, local heat-transfer measurements were made at approximately 850 points on the surface of the test plate for a wide range of plate orientations and Reynolds numbers. From the standpoint of fundamentals, this information reveals the various transport mechanisms that are operative. Furthermore, the local distributions clearly show where the zones of highest and lowest heat transfer occur on the plate surface. Armed with this information, it is possible to suggest ways of reducing the overall heat transfer from the surface to the airstream. Such a reduction, if realized, would have practical benefits—for example, in increasing the efficiency of a flat plate solar collector.

The pattern of fluid flow adjacent to the plate is three dimensional and of a complex nature. In particular, depending on the orientation of the plate, there may be a stagnation region on the surface which is framed by a region of outward radiating streamlines. A knowledge of the flow pattern is of considerable benefit in the interpretation of the local heat-transfer distribution. To determine the flow patterns, the oil/lampblack flow visualization technique was employed. The resulting flow-pattern traces were recorded photographically and are presented here. Especially noteworthy among these photographs is the chronicle of the movement and the change of shape of the stagnation region as the plate's orientation is varied from normal to various inclinations relative to the flow.

In addition to the aforementioned local results, measurements of average transfer coefficients were also made to extend the range already investigated in [1]. The extended range encompassed a set of plate–airstream orientations different from those of [1]. These additional measurements were undertaken to verify the breadth of applicability of the data correlation given there.

The actual experiments were performed with mass transfer rather than with heat transfer, and the mass-transfer coefficients were converted to heat-transfer coefficients via the well-established analogy between the two processes. Specifically, the mass-transfer experiments involved the sublimation of naphthalene. The advantages of the naphthalene sublimation technique, relative to direct heat-transfer experiments, lie in the easier attainment of boundary condition uniformity, absence of extraneous losses via structure and supports, and generally higher accuracy. The heat-transfer boundary condition analogous to that of the mass-transfer experiments is uniform wall temperature.

A square plate was used in all the experiments. It was mounted in the test section of a low turbulence wind tunnel. The mounting fixture enabled the orientation of the plate to be varied relative to the airstream, and the specification of the angular coordinates defining the orientation will be discussed shortly. The overall range of the Reynolds number extended from about 20 000 to 120 000.

THE EXPERIMENTS

Apparatus

The naphthalene plates employed in the experiments were made by a casting process. Molten naphthalene was poured into a stainless steel mold consisting of a highly polished flat plate and a hollowed-out block. Upon separation of the mold parts, the naphthalene face formed adjacent to the polished plate was exposed, and it is this face that served as the mass-transfer test surface. Aside from this exposed face, the rest of the naphthalene casting remained housed in the hollowed-out block, which thereby served the function of a cassette.

The cassette was subsequently mounted in the wind tunnel and oriented so that the exposed naphthalene surface faced the airflow. The edges of the cassette were beveled to ensure that the oncoming flow would not be diverted by edge bluntness.

When viewed head-on, the naphthalene test surface may be seen to be framed by a thin border which is part of the cassette. The naphthalene surface and its framing border constituted a square with a 7.62 cm (3 in) side. The border was 0.238 cm (3/32 in) in width. A photographic view of the naphthalene plate and cassette in place in the wind tunnel is given in Fig. 2 of [1], and the mold is shown in Figs. 3 and 4 therein. Further information about the casting procedure and the naphthalene test surface and its cassette is available in [1] and [2]. A new naphthalene plate was cast for each data run.

The back side of the cassette (i.e. the leeward side) was equipped with a fixture which facilitated adjustment of the orientation of the naphthalene surface relative to the direction of the oncoming airflow. Two sets of angles were employed to describe the orientation. For the experiments reported in [1], the orientation angles were denoted by α and ϕ and respectively designated as angle of attack and angle of yaw. These angles are illustrated in Fig. 1. In the uppermost diagram of Fig. 1, the plate is shown in a reference orientation in which the naphthalene surface is normal to the oncoming flow. An orthogonal X,Y,Z coordinate system is centered on the plate, with the wind aligned with $X0$. The line $0A$ is a reference line. The angle α is set by a rotation of the plate around $0Y$ (middle diagram), and the angle ϕ by a rotation about the normal $\hat{n}$ to the plate surface. Note that normal impingement is characterized by $\alpha = 90°$, $\phi = 0°$.

Whereas these angles constitute an acceptable means of specifying the orientation of the surface, it

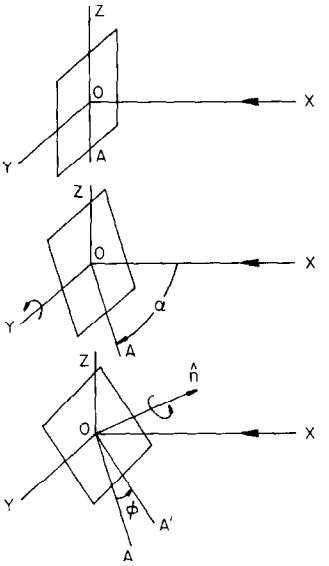

FIG. 1. Description of the plate orientation in terms of the angles of attack and yaw $-\alpha$ and ϕ.

was pointed out to the authors that they are different from the standard orientation angles used in aerodynamics. These standard angles, pitch and yaw, are illustrated in Fig. 2 and are denoted by α' and ϕ' (to make them distinct from α and ϕ). The upper diagram of Fig. 2 portrays the reference orientation (normal impingement). As indicated in the middle diagram, the pitch angle α' is set by a rotation about $0Y$ in a manner similar to the setting of α. Now, however, the yaw angle ϕ' is obtained by rotation about the $0Z$ axis as illustrated in the lower diagram.

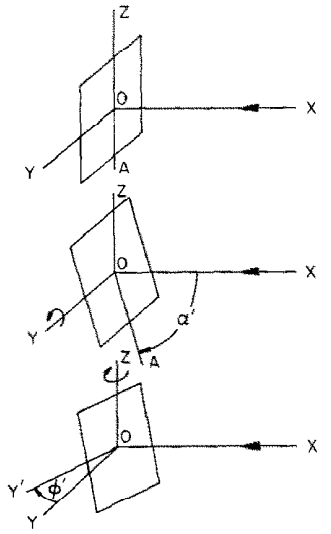

FIG. 2. Description of the plate orientation in terms of the angles of pitch and yaw—α' and ϕ'.

It is evident that the same pair of values assigned to α,ϕ and to α',ϕ' will, in general, yield different orientations. To avoid confusion, we will use the designation attack/yaw when referring to an α,ϕ orientation and pitch/yaw when referring to an α',ϕ' orientation.

As noted earlier, the α,ϕ angles were employed to parameterize the average coefficients reported in [1]. In the present research, average coefficients parameterized by α',ϕ' were measured and are compared with those of [1]. Furthermore, the local coefficients and fluid flow patterns will be parameterized by the α',ϕ' angles. The experiments were performed for α and α' between 90 and 25° and for ϕ and ϕ' between 0 and 45°. The overall range of the Reynolds number extended from about 20000 to 120000.

The test plate was fitted with a pair of thermocouples that were embedded in the naphthalene just below its exposed surface (the thermocouples were threaded through the rear of the cassette). Readings of these thermocouples were recorded at 2 min intervals during each data run. At any instant, the readings of the two thermocouples never differed by more than 0.03°C (0.05°F). The temperature of the airstream was also recorded periodically. The velocity in the test section of the wind tunnel was measured with an L-shaped impact tube in conjunction with a wall static tap.

The cross section of the wind tunnel test section was a 61×30.5 cm (2×1 ft) rectangle. Operation of the tunnel was in the open-circuit mode, with the naphthalene-laden air discharged out of doors. The velocities available in the test section ranged from 4.5 to 24 m/s (15 to 80 ft/s). Over this range, the turbulence level was about 0.2%.

Experimental procedure

A general description of the experimental procedure employed in determining the overall transfer coefficients is presented in [1], and this same procedure was followed here. In view of the fact that the vapor pressure of naphthalene, the driving force for the mass transfer, is quite sensitive to temperature (10% change per 1°C), precautions were taken to ensure the attainment of a known, steady plate temperature. Care was also exercised to minimize and correct for any uncertainties in mass transfer during the set-up and disassembly of the experiment. Aside from these special (and essential) procedures [1, 2], the steps in an average-coefficient data run included an initial weighing of the test element (i.e. the naphthalene plate and its cassette), installation of the test element in the wind tunnel and exposure to the airstream for a preselected time, removal of the element from the tunnel followed by a final weighing.

The weighings were accomplished with a Mettler analytical balance with a capacity of 200 g and a smallest scale reading of 0.1 mg. The net mass transfer during a typical data run was about 180 mg, which corresponds to an average surface recession of 0.0025 cm (0.001 in). Run times were in the range from 40 to 75 min.

The experimental procedure for the determination of the local transfer coefficients encompassed all aspects of the average-coefficient experiments plus the local measurements that will now be described. The local mass transfer rates were deduced from measurements of the surface contour of the naphthalene plate both before and after a data run. These measurements were performed with the naphthalene surface mounted face up on a movable, horizontal coordinate table which enabled two directions of horizontal travel. The table was equipped with a special fixture which mated with an interlocking member on the back side of the cassette. The contour measuring instrumentation was affixed to a strut which overhung the coordinate table.

The depth profiles were determined with the aid of instrumentation which converts the movement of a sensor tip (similar to the tip of a dial gage) into an electrical signal that can be read and recorded by a digital voltmeter. The instrumentation includes a sensing head which houses a linear variable differential transformer and signal conditioning electronics. The sensing arrangement is capable of resolving surface elevations to within 2.54×10^{-5} cm (10^{-5} in).

A measurement sequence was established whereby the elevations were sensed over a grid of 29×29 points (i.e. 841 points) on the naphthalene surface.

The points were equally spaced except near the edges where a finer spacing was employed. In addition to the measurements on the naphthalene, elevations were also measured on the stainless steel frame which surrounds the naphthalene plate. The latter measurements were made to provide reference points to facilitate the data reduction (the use of these reference points will be discussed shortly). The elevation measurements on the naphthalene surface and on the frame were made both before and after a data run. In addition, auxiliary measurements were carried out in a typical case to determine the influence of natural convection sublimation during the period of time when the surface contour measurements were being made.

To detect the pattern of fluid flow over the plate, a flow visualization study was undertaken using the oil/lampblack technique. According to this technique, the test surface is coated with a thin film of a lampblack and oil mixture and then exposed to the airflow. The consistency of the mixture must be such that it flows readily under the action of the shear stresses exerted by the air on the surface. However, the mixture should not be so fluid that it would all be blown off the surface. Therefore, different oils (i.e. different viscosities) and/or proportions of oil and lampblack have to be used to accommodate the varying level of shear stress with Reynolds number. At higher Reynolds numbers, a stiffer mixture is appropriate, while a more fluid mixture is suitable at lower Reynolds numbers.

In the present experiments, the requisite fluidity was obtained by use of oils of different viscosity, respectively a red manometer oil for the higher Reynolds numbers and a light petroleum distillate (i.e. rust penetrating oil) at the lower Reynolds numbers. The weight proportion of oil and lampblack was 12 to one. To provide a highly contrasting background for the oil/lampblack mixture and to enable consecutive runs to be made without concern about degradation of surface quality, a sheet of white (plastic-coated) contact paper was cemented to the test surface.

Photographs of the flow pattern traces were taken with the plate removed from the wind tunnel, and side lighting by floodlights was employed to attain greater sharpness. Tri-X film was used for all the photographic work.

DATA REDUCTION

The evaluation of the average transfer coefficients follows a pattern that was already described in [1] and which needs only brief review here. From the mass measurements before and after the data run and from the timed duration of the run, the average mass-transfer rate $\dot{M}$ is determined. Then the average mass-transfer coefficient $\bar{K}$ is evaluated:

$$\bar{K} = (\dot{M}/A)/(\rho_{nw} - \rho_{n\infty}), \tag{1}$$

where A is the face area of the naphthalene plate, and ρ_{nw} and $\rho_{n\infty}$ are, respectively, the naphthalene vapor concentrations at the plate surface and in the free stream. The latter is zero in the present experiments and the former can be calculated from the Sogin [3] vapor pressure–temperature relationship in conjunction with the perfect gas law.

For a dimensionless presentation, the Colburn j-factor is used:

$$j = (\bar{K}/U_\infty)Sc^{2/3}, \tag{2}$$

in which Sc is the Schmidt number (equal to approximately 2.57 in the present experiments). According to the analogy, the j-factors for heat and mass transfer are equal, where the former is defined as:

$$j = StPr^{2/3}, \quad St = \bar{h}/\rho c_p U_\infty. \tag{3}$$

The j-factor results will be presented as a function of the Reynolds number Re:

$$Re = U_\infty S/\nu, \tag{4}$$

with S as the side of the square plate (i.e. the outside dimension of the frame).

The determination of the local transfer coefficients and their subsequent representation in terms of contour lines involved a lengthy procedure. To begin, the before and after elevation measurements at each of the 841 points on the naphthalene surface were differenced. These differences were then modified in accordance with the repositioning correction. The need for this correction stems from the fact that there are, necessarily, slight changes in surface elevation inherent in removing and repositioning the naphthalene plate on the coordinate table. The repositioning correction was made by employing the measured elevations of reference points situated on the stainless steel border that frames the naphthalene plate. Since these points do not participate in the mass-transfer process, any measured changes in their elevations can be attributed to repositioning.

The detailed implementation of the repositioning correction is described in [2]. The accuracy of the correction procedure is supported by the closure of the overall mass balance. For each data run, such a mass balance was evaluated by comparing the overall mass transfer obtained by direct weighing with that from a numerical integration of the local mass transfer distribution. Typically, the closure was within 5%.

Once the repositioning corrections had been applied to the local elevation changes and the average elevation change determined by integration, each of the local changes was ratioed with the average. This operation yielded, at each measurement station, the ratio of the local mass-transfer coefficient to the average mass-transfer coefficient. This ratio may be denoted by $K/\bar{K}$ or analogously by $h/\bar{h}$. Then, working graphs were prepared in which $K/\bar{K}$ was plotted against one of the surface coordinates for parametric values of the other surface coordinate. These graphs were then entered

with a preselected value of $K/\bar{K}$, and the coordinates were read at the points at which this $K/\bar{K}$ value was encountered. The coordinates were employed to plot contour diagrams portraying lines of constant $K/\bar{K}$. These contour diagrams will be presented later.

The extraneous sublimation by natural convection during the period of surface contour measurement was sufficiently small so as not to affect the contour diagrams.

RESULTS AND DISCUSSION

Average coefficients

The average mass-transfer coefficients will be presented in dimensionless form in terms of the j-factor. This representation enables the mass-transfer results to be employed in heat-transfer applications in accordance with equation (3).

The j-factors measured during the present investigation will now be compared with those of [1]. The plate orientations of the present experiments encompassed pitch angles α' of 90, 65, 45 and 25° and yaw angles of ϕ' of 0, 22.5 and 45°. In [1], the angle of attack α was assigned values of 90, 65, 45 and 25° with yaw angles ϕ of 0, 22.5 and 45°. As noted earlier and can be verified from Figs. 1 and 2, the pitch/yaw specification generally yields different orientations than does the attack/yaw specification when $\alpha' = \alpha$ and $\phi' = \phi$.

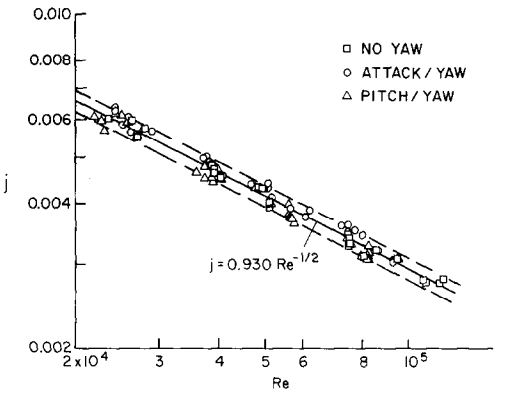

FIG. 3. Average heat- (or mass-) transfer coefficients.

The results from the two investigations are brought together in Fig. 3, where j is plotted as a function of the Reynolds number on log–log coordinates. Three types of symbols are used to distinguish the data. The no-yaw data (squares) are common both to the present investigation and to [1] (i.e. $\phi' = \phi = 0$). The circles designate the attack/yaw data of [1] for nonzero yaw, while the triangles represent the present pitch/yaw data for nonzero yaw. Note that specific parameterization of the data with regard to the particular values of α,ϕ and α',ϕ' is not indicated in Fig. 3 (this information is available in [2]). The omission of such a parameterization is a logical consequence of the insensitivity of the results to the specifics of the plate orientation.

A least-squares straight line of the form $j = \text{const.}/Re^{1/2}$ has been passed through the data, with the result:

$$j = 0.930/Re^{1/2}. \tag{5}$$

This equation is portrayed by a solid line in Fig. 3, and dashed lines displaced from it by $\pm 5\%$ are also shown. From an inspection of the figure, it can be seen that almost all of the data fall within $\pm 5\%$ of the correlating line. Therefore, for almost all practical purposes, the overall coefficients can be regarded as independent of the plate orientation within the broad range that has been investigated.

The aforementioned insensitivity was already noted in [1], but that observation was confined to attack/yaw orientations. The present investigation has added another set of orientations (i.e. the pitch/yaw orientations), and the insensitivity has been shown to persist—thereby re-enforcing its generality.

If detailed observations are made in Fig. 3, then a pattern can be identified whereby the circles generally fall above the average, the squares fall along the average, and the triangles fall below the average. Furthermore, by making use of the graphs of [2], a fine-grained pattern within each data set can be identified. Thus, what appears to be data scatter in Fig. 3 is, at least in part, a parametric variation of the results with orientation. These variations are, however, of second order importance. Furthermore, they are of such small scale that their occurrence is difficult to explain.

Before leaving this section, it may be noted that the attack/yaw data of Fig. 3 correspond to the repeat runs cited in the addendum of [1].

Fluid flow patterns

As was discussed earlier, the patterns of fluid flow adjacent to the plate surface were made visible by employing the oil/lampblack technique. Under the action of the shear stresses exerted by the air on the surface, an initially uniform film of a mixture of oil and lampblack is moved along the surface in the flow direction. The result is a pattern of streaks which reveal the flow path of the air as it passes over the surface. In a stagnation region, the oil and lampblack mixture remains as it was initially applied, so that a black region without streaks is indicative of stagnation conditions.

The flow visualization studies were carried out for two Reynolds numbers, 79 000 and 33 000. In general, the streak line patterns were sharper at the higher Reynolds number than at the lower Reynolds number. This is because the greater shear forces at the higher Reynolds number enabled a stiffer, gravity-resistant mixture to be used. At the lower Reynolds number, a compromise mixture fluidity had to be found which would enable the mixture to respond to the lesser surface shear stresses while, at the same time, resisting gravity. As a result of this compromise, the streak lines were somewhat less sharp.

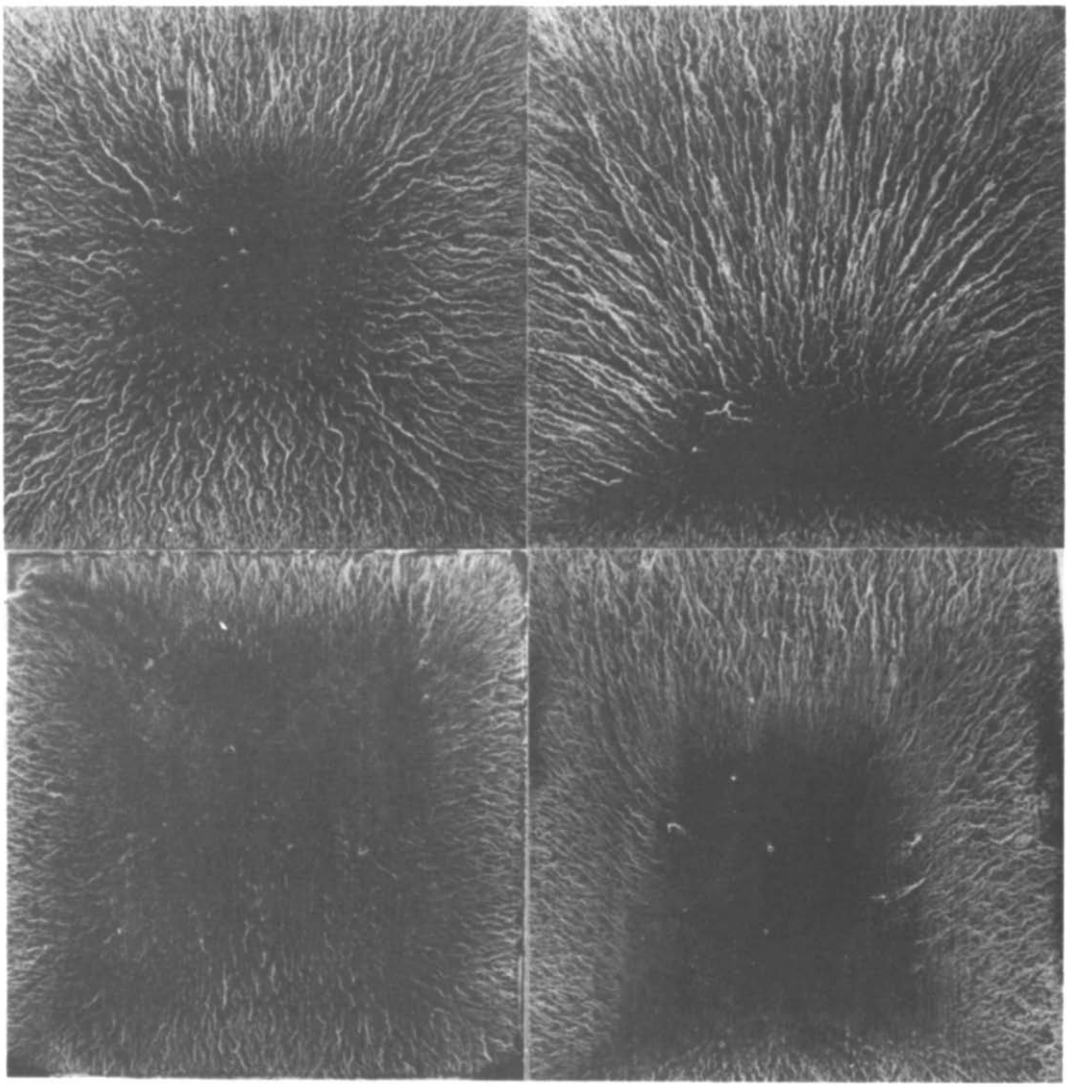

FIG. 4. Fluid flow patterns for zero yaw and for pitch angles of 90° (left) and 60° (right). The upper and lower photographs are for $Re = 79\,000$ and 33 000, respectively.

The plate orientations for the visualization studies encompassed pitch angles α' of 90, 60, 40 and 25°, and at each of these pitch angles runs were made for yaw angles of ϕ' of 0, 22.5 and 45°. Owing to journal space limitations, only a selection of the flow visualization photographs can be included here, but the full set is available in [2].

In interpreting the results, it should be noted that the photographs correspond to a head-on view of the plate surface. For pitch angles less than 90°, the lower edge of the plate is thrust forward into the direction of the oncoming flow (as illustrated in Fig. 2). Similarly, for yaw angles greater than 0°, the right-hand edge of the plate is thrust forward, again as illustrated in Fig. 2.

Attention will first be turned to the results for zero yaw as presented in Figs. 4 and 5. The first of these is for pitch angles α' of 90 and 60°, while the second is for α' of 40 and 25°. For each angle, the photos for the two Reynolds numbers (79 000 and 33 000) are placed one above the other.

When the plate is situated normal to the flow ($\alpha' = 90°$), there is a stagnation zone in the central region of the plate with a surrounding region of radial outflow. As the plate is inclined and α' decreases, the stagnation zone progressively moves forward and ultimately coincides with the forward-thrusted leading edge. Although the movement of the stagnation zone is the most apparent outcome of the inclination of the plate, there are a number of other interesting flow field features that will be identified and discussed.

At $\alpha' = 60°$, the stagnation zone has a somewhat triangular shape and tends to be broader at its forward edge than at its rearward edge. Forward of the stagnation zone, the flow adjacent to the plate moves upstream toward the leading edge, even though the freestream flow moves downstream. This upstream flow can be regarded as a legacy of the $\alpha' = 90°$ case. Furthermore, there is a substantial amount of sidewise motion, so that the flow is strongly three-dimensional.

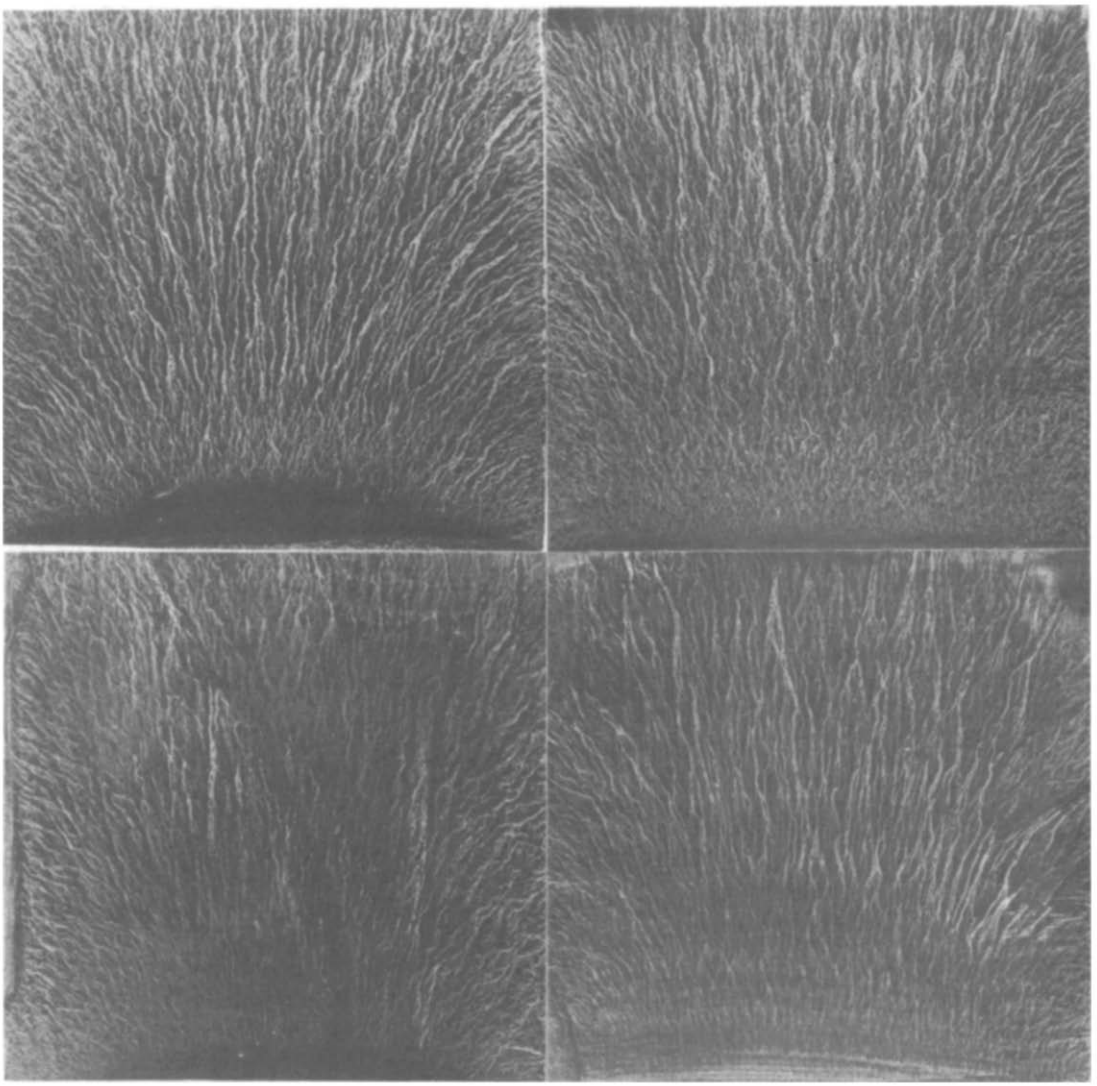

FIG. 5. Fluid flow patterns for zero yaw and for pitch angles of 40° (left) and 25° (right). The upper and lower photographs are for $Re = 79\,000$ and 33 000, respectively.

As α' is decreased to 40°, the stagnation zone takes the form of a band adjacent to the leading edge. Careful inspection of Fig. 5 reveals a narrow residual region of upstream flow between the forward edge of the stagnation zone and the leading edge. It also appears that there is a tendency toward more longitudinal and less sidewise flow. This tendency is even more in evidence at $\alpha' = 25°$, where strong sidewise flows appear to be confined adjacent to the side edges of the plate. Furthermore, the stagnation zone appears to have become coincident with the leading edge of the plate.

Consideration may now be given to the effects of yaw on the fluid flow patterns. The yawing of the plate at 90° pitch provides orientations that are identical to those obtained by varying the pitch at 0° yaw. Therefore, by turning the photographs of Figs. 4 and 5 so that the lower edge becomes the right-hand edge, the flow patterns of those figures represent those for 90° pitch and varying degrees of yaw.

The interaction of yaw ($> 0°$) and pitch ($< 90°$) will now be illustrated in Figs. 6 and 7. Figure 6 corresponds to 60° pitch and yaw angles of 22.5 and 45°, and Fig. 7 is for 25° pitch and the same yaw angles. In Fig. 6, the 60° pitch, 22.5° yaw combination represents nearly the same degree of pitch and yaw displacement from the 90° pitch, 0° yaw orientation. Therefore, the flow pattern is more or less symmetric around the diagonal extending from the lower right to the upper left. The stagnation zone is centered near the right-hand corner. Adjacent to both the right-hand and lower edges, there are flows which are directed from the interior of the plate toward the respective edge.

The 60° pitch, 45° yaw case of Fig. 6 represents a stronger yaw displacement than pitch displacement. As a consequence, the stagnation zone is concentrated along the right-hand edge of the plate. A further evidence of the dominance of yaw is that the flow is strongly transverse over most of the plate.

In Fig. 7, the stagnation region is seen to coincide

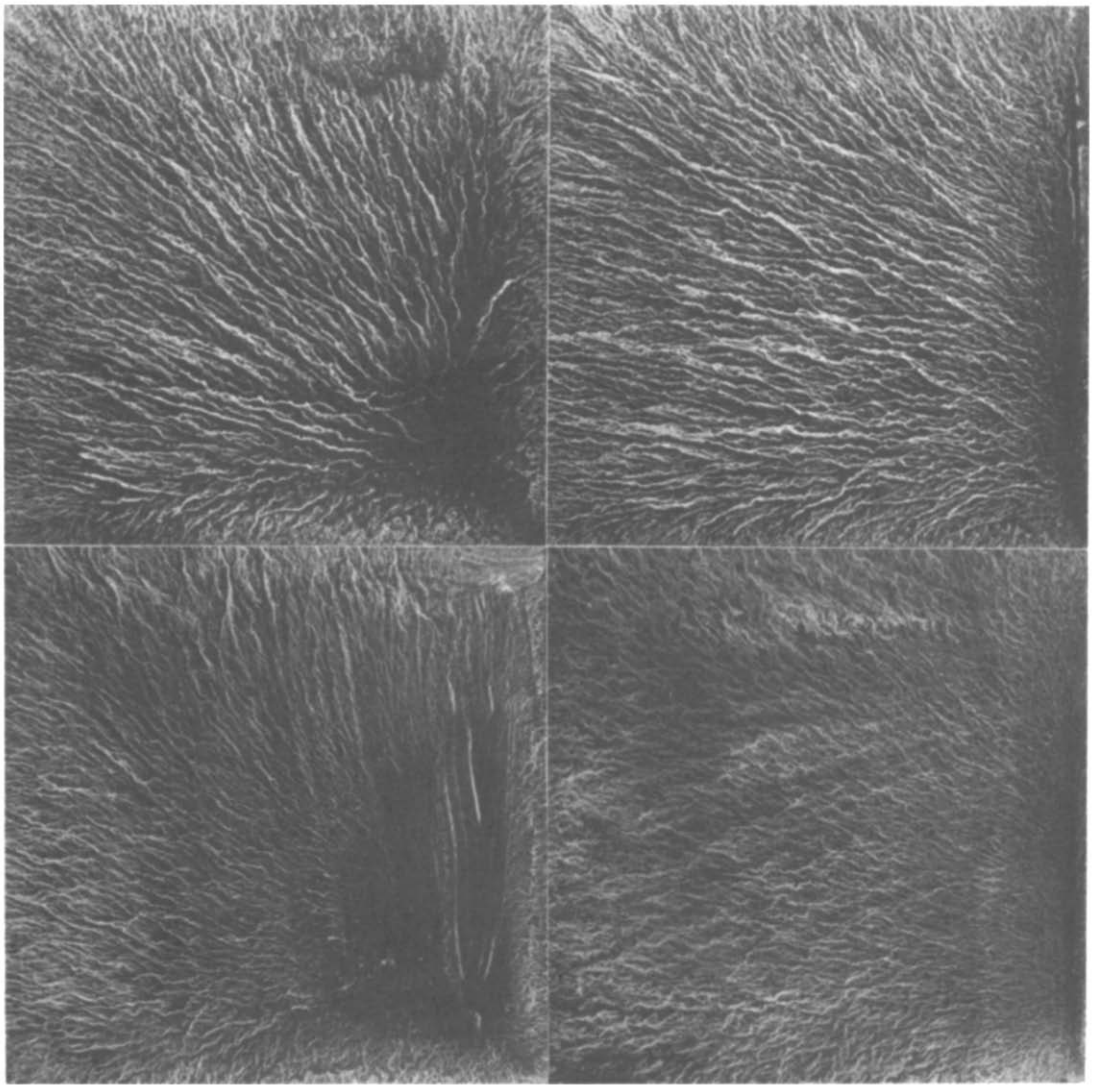

FIG. 6. Fluid flow patterns for 60° pitch and for yaw angles of 22.5° (left) and 45° (right). The upper and lower photographs are for $Re = 79\,000$ and 33 000, respectively.

with the leading edge. The 25° pitch dominates over the 22.5° yaw, so that the streak lines in the left-hand photographs have a strong longitudinal component. On the other hand, the greater yawing of the plates in the right-hand photos introduces a significant transverse component.

If Figs. 4–7 are viewed globally, it is evident that a wide spectrum of flow patterns are encountered as the orientation of the plate is varied. In this light, the relative insensitivity of the overall heat- (mass-) transfer coefficients to orientation appears quite remarkable. Another noteworthy finding of the visualization studies is the complexity of the flow field, the degree of which can be gauged by comparison with the purely longitudinal streak lines of two-dimensional boundary-layer flow. It may also be observed that, by and large, the flow patterns are not very sensitive to the Reynolds number over the range investigated, although there are some differences in detail.

Local heat-/mass-transfer coefficients

The distribution of the local heat- (or mass-) transfer coefficient on the plate surface will be presented via contour diagrams in which lines of constant $h/\bar{h}$ (or $K/\bar{K}$) are plotted. Such contour diagrams have been prepared from data for pitch angles of 90, 60 and 25° and yaw angles of 0 and 45°, with nominal Reynolds numbers of 25 000 and 80 000. The 60°-pitch results are not included here because of space limitations but can be found in [2]. The results for the other cases are presented in Figs. 8–11. Each of these figures is for a given orientation and contains two graphs, respectively for the two Reynolds numbers. Figures 8 and 9 are for the no-yaw case and illustrate the effect of varying the pitch angle from 90 to 25 . The interaction between pitch (< 90) and yaw (> 0) is shown in Figs. 10 and 11.

The discussion will first be focused on the results for a plate situated normal to the flow ($\alpha' = 90°$, $\phi' = 0°$), Fig. 8. Owing to symmetry, only half of the

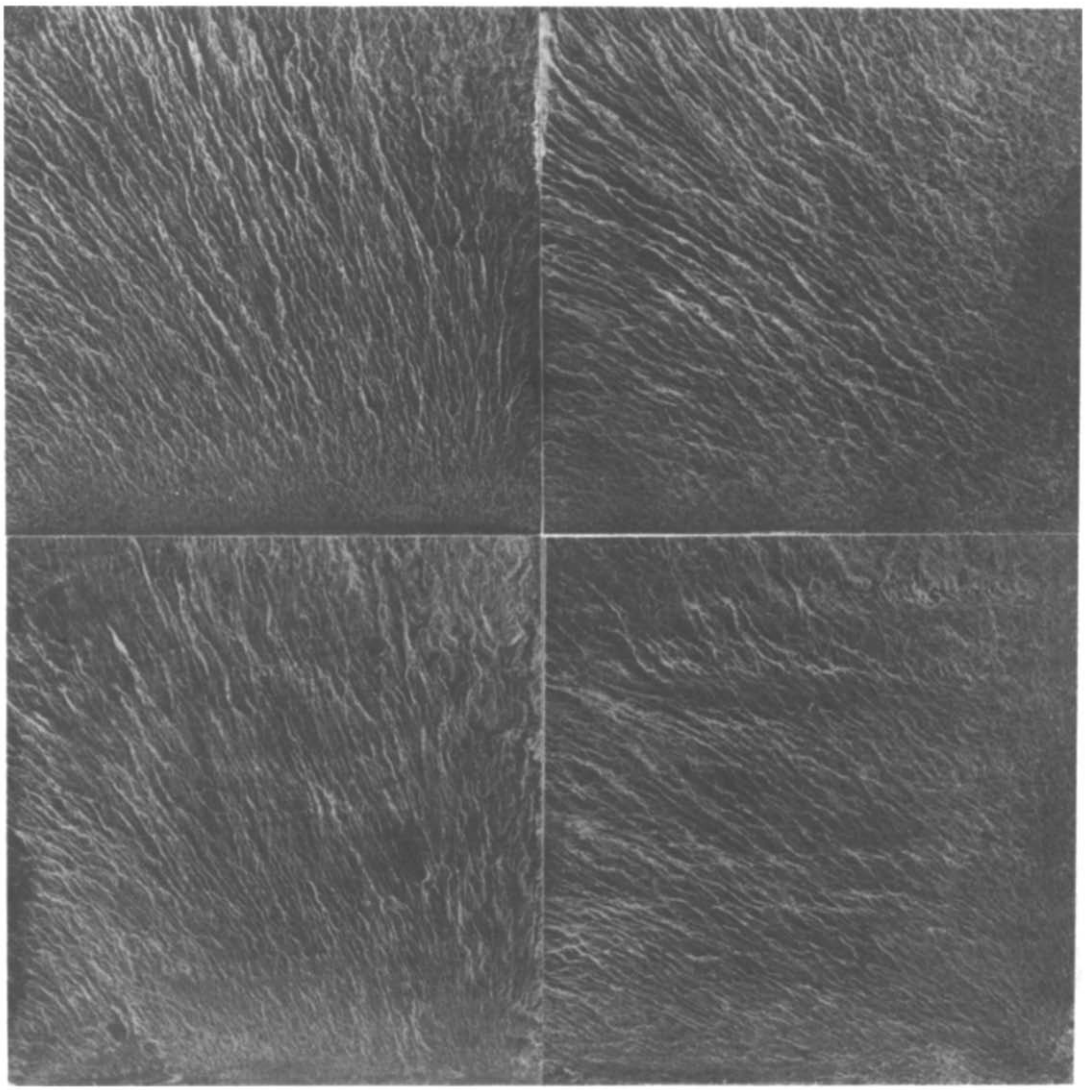

FIG. 7. Fluid flow patterns for 25° pitch and for yaw angles of 22.5° (left) and 45° (right). The upper and lower photographs are for $Re = 79\,000$ and 33 000, respectively.

plate is shown in each of the graphs presented in the figure. Inspection of the figure reveals that the lowest heat-transfer coefficients occur in the central region of the plate, and that the coefficients increase in the radial direction from the center to the edges. Since the central region has already been identified as a stagnation zone (Fig. 4), it follows that the lowest transfer coefficients occur in the stagnation region.

At first encounter, this finding appears to be at variance with expectations about stagnation regions. These expectations are based on prior experience with such well-known cases as the forward stagnation points of cylinders and spheres in crossflow. In those cases, the boundary-layer thickness increases with increasing distance from the stagnation point, thereby causing a decrease in the heat-transfer coefficient. In the present instance, the boundary-layer thickness decreases from the center of the plate toward the edges, and the transfer coefficient increases. The decrease in the boundary-layer thickness appears quite plausible when it is realized that the radially outflowing streamlines are pressed toward the surface by the freestream flow which passes beyond the edges of the plate.

The inclining of the plate to a 25° pitch (Fig. 9) alters the contour line pattern to some extent, but retains the basic characteristic that the highest coefficients occur near the edges. Owing to the inclination, the fore–aft symmetry of Fig. 8 is not perpetuated in Fig. 9; instead, higher coefficients are in evidence in the fore part of the plate than in the aft part. In view of the markedly different patterns of fluid flow in the two cases (see Figs. 4 and 5), the rationalization of the transfer coefficients of Fig. 9 is markedly different from that for the coefficients of Fig. 8.

First of all, the stagnation region now coincides with the leading edge and, therefore, does not play a significant role. The high transfer coefficients that occur in the forward part of the plate are due to the

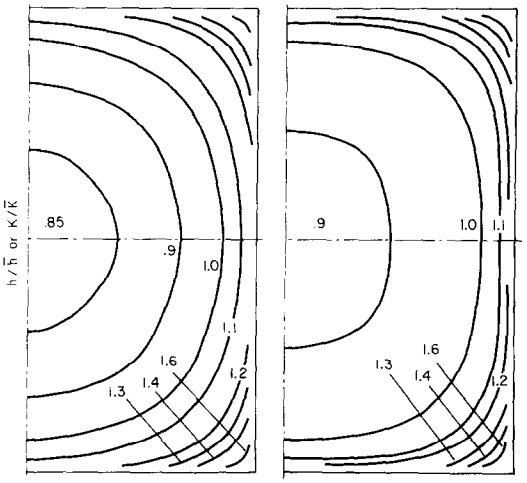

FIG. 8. Contour lines of constant local heat- (or mass-) transfer coefficient for a plate situated normal to an oncoming flow ($\alpha' = 90°$, $\phi' = 0°$). $Re = 80\,000$ (left) and 22 000 (right).

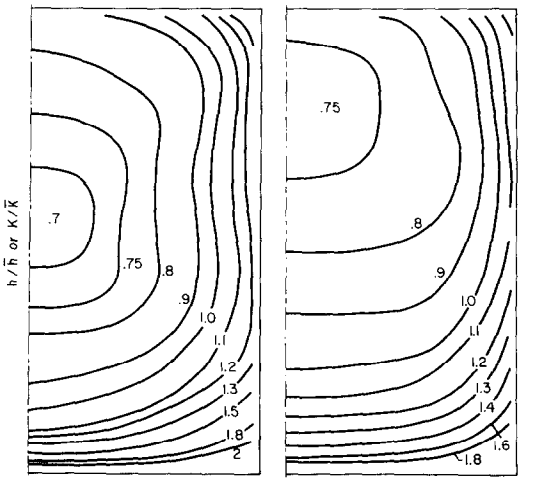

FIG. 9. Contour lines of constant local heat- (or mass-) transfer coefficient for zero yaw and for 25° pitch. Re = 85 000 (left) and 28 000 (right).

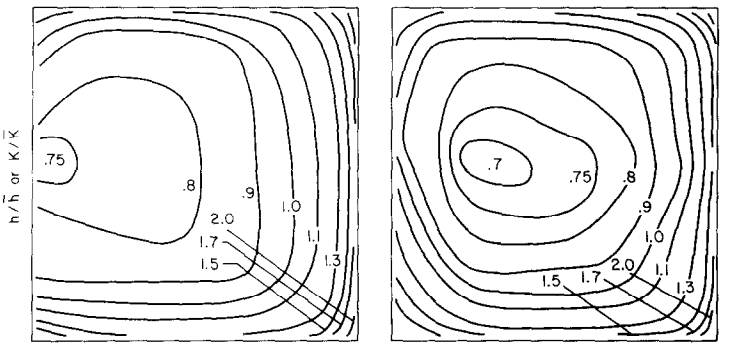

FIG. 10. Contour lines of constant heat- (or mass-) transfer coefficient for 60° pitch and 45° yaw. Re = 77 000 (left) and 25 000 (right).

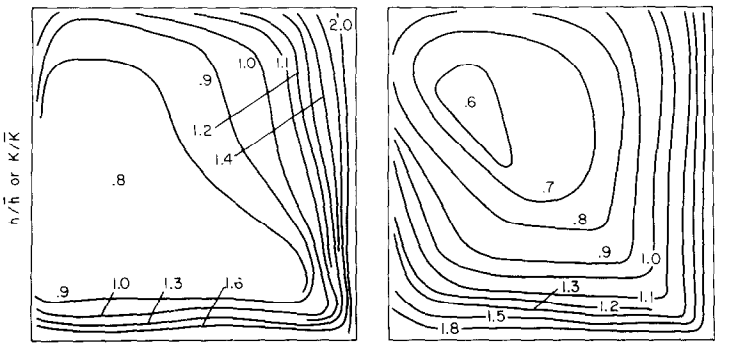

FIG. 11. Contour lines of constant heat- (or mass-) transfer coefficient for 25° pitch and 45° yaw. Re = 82 000 (left) and 26 000 (right).

developing boundary layer, and the decrease of the coefficients along the plate reflects the growth of the boundary-layer thickness. The decrease is arrested and ultimately reversed by two factors. First, the boundary-layer growth is slowed by the escape of fluid toward the side edges of the plate. Second, as the rear edge (i.e. the trailing edge) is approached, the streamlines are pressed toward the surface by the freestream flow that passes beyond the edge. The relatively high transfer coefficients that occur adjacent to the side edges of the plate are also due to thinning of the boundary layer. This thinning has been experimentally demonstrated [4, 5] for flow along a flat plate aligned with the free stream and should also occur (perhaps to even a greater extent) for inclined plates.

The results for interacting pitch and yaw will now be discussed. For the 60°-pitch, 45°-yaw orientation, the visualization photos of Fig. 6 show a strongly yaw-influenced flow which moves more or less transversely over the plate from right to left, with the right-hand edge serving as the leading edge. This flow pattern is mirrored by the contour lines of Fig. 10, where the influence of the developing boundary layer adjacent to the right-hand edge is evidenced by the high transfer coefficients which decrease in the flow direction. The relatively high coefficients adjacent to the top and bottom edges are consistent with the expected thinning of the boundary layer as discussed at the end of the last paragraph. It might also be expected that the trailing edge (i.e. the left-hand edge) would be a zone of relatively higher coefficients. This expectation is realized at the lower of the two Reynolds numbers, but not at the higher.

For the 25°-pitch, 45°-yaw orientation, Fig. 7 indicates a more or less diagonal flow with both the right-hand and bottom edges serving as leading edges. The distribution of heat-transfer coefficients for this case (Fig. 11) is consistent with this flow pattern. High transfer coefficients which decrease in the flow direction are in evidence along both the right-hand and bottom edges.

With the aid of the flow visualization photographs, most of the main characteristics of the local heat-transfer results of Figs. 8–11 can thus be rationalized. However, the inconsistent behavior of the coefficients in the neighborhood of the trailing edge makes it difficult to formulate a complete explanation of all of the observed characteristics.

APPLICATIONS AND CONCLUDING REMARKS

It is interesting to assess the impact of the results on the applications that motivated this work—specifically, the wind-related heat loss from a flat plate solar collector. With regard to the average heat-transfer coefficients, the enlarged range of plate orientations investigated here has lent further support to the generality of equation (5) as a computational tool for assessing collector heat losses. It should be recognized, however, that the equation is based on square-plate experiments, so that further work is needed to assess its applicability to collectors of rectangular planform.

The results for the local heat-transfer coefficient convey information that is of potential practical utility for solar collectors. These results show that relatively high values of the transfer coefficient occur adjacent to the edges of the plate. If these high coefficients were to be deactivated, then the overall heat loss could be diminished. Inasmuch as hydrodynamic edge effects contribute significantly to these high coefficients, it would appear that the thermal losses could be reduced if the hydrodynamic edges of the plate were to extend beyond the thermally active portion of the plate. In practice, for example, such extensions could be a portion of a roof on which a collector was mounted. To examine the possible reductions of the overall heat-transfer coefficient, it remains to perform experiments on plates in which the thermally active portion is framed by co-planar thermally passive extensions.

Acknoledgement—This research was performed under the auspices of NSF Grant ENG77-06762.

REFERENCES

1. E. M. Sparrow and K. K. Tien, Forced convection on an inclined and yawed flat plate—application to solar collectors, *J. Heat Transfer* **99**, 507–512 (1977).
2. K. K. Tien, Heat/mass transfer characteristics and fluid flow patterns for airflow about an inclined and yawed flat plate, Ph.D. Thesis, Department of Mechanical Engineering, University of Minnesota, Minneapolis, Minnesota (1978).
3. H. H. Sogin, Sublimation from disks to air streams flowing normal to their surfaces, *Trans. Am. Soc. Mech. Engrs* **80**, 61–69 (1958).
4. J. W. Elder, The flow past a flat plate of finite span, *J. Fluid Mech.* **9**, 133–153 (1960).
5. E. B. Davies and A. D. Young, Streamwise edge effects in the turbulent boundary layer on a flat plate of finite aspect ratio, Aero. Res. Coun. Gt. Britain, Reports and Memoranda No. 3367 (1963).

TRANSFERT THERMIQUE LOCAL ET CARACTERISTIQUES DYNAMIQUES POUR UN ECOULEMENT D'AIR NORMAL OU NON A UNE PLAQUE CARREE

Résumé—Des expériences en soufflerie permettent de déterminer les coefficients locaux ou moyens de transfert thermique et les configurations de l'écoulement pour une plaque carrée avec différentes orientations par rapport à l'écoulement principal. On emploie le technique de sublimation du naphtalène pour la détermination des coefficients de transfert et les configurations de l'écoulement proche de la plaque sont visualisés par la technique du noir de fumée. Les orientations de la plaque utilisées pour les mesures du coefficient moyen élargissent le domaine antérieurement étudié et les résultats de ces mesures affirment l'insensibilité du coefficient moyen à l'orientation. Les coefficients locaux de chaleur (ou de masse) sont présentés par des diagrammes avec des courbes de valeurs constantes. En général, les plus grands coefficients sont situés près des bords de la plaque. Ces coefficients élevés sont étroitement couplés aux phénomènes hydrodynamiques qui concernent non seulement la couche limite classique de bord de fuite, mais aussi d'autres mécanismes reliés à la dimension finie de la plaque. Pour une plaque normale à l'écoulement, le plus faible coefficient se trouve situé au centre de la région d'arrêt et le coefficient croît du centre vers les bords. L'écoulement est tridimensionnel et très complexe. Un des résultats intéressants est que la région de stagnation migre depuis la position centrale, pour l'incidence normale, vers une position plus avancée lorsque la plaque est inclinée.

LOKALER WÄRMEÜBERGANG UND STRÖMUNGSFORMEN BEI SCHRÄGER ODER SENKRECHTER ANSTRÖMUNG EINER QUADRATISCHEN PLATTE

Zusammenfassung—Es wurden Windkanal-Versuche durchgeführt, um die lokalen und mittleren Wärmeübergangskoeffizienten sowie die Strömungsformen an einer quadratischen Platte zu bestimmen, die in unterschiedlichen Neigungen zur Strömungsrichtung angebracht war. Die Naphthalin-Sublimationsmethode wurde zur Bestimmung der Wärmeübergangskoeffizienten angewandt. Die Strömungsformen wurden mit Hilfe von Olruß sichtbar gemacht. Die Neigungen der Platte, bei denen die mittleren Koeffizienten gemessen wurden, überschritten den früher untersuchten Bereich. Die Ergebnisse dieser Messungen bestätigten die Unempfindlichkeit der mittleren Koeffizienten gegen Änderungen der Orientierung. Die lokalen Wärme- (oder Stoff-) übergangskoeffizienten sind in Konturdiagrammen dargestellt, in denen die Linien konstanter Koeffizienten aufgetragen sind. Im allgemeinen treten die höchsten Wärmeübergangskoeffizienten in der Nähe der Plattenecken auf. Diese hohen Koeffizienten sind eng verbunden mit den hydrodynamischen Erscheinungen, die an den Ecken auftreten. Diese Erscheinungen beinhalten nicht nur die konventionelle Randgrenzschicht, sondern auch Vorgänge, die mit der endlichen Größe der Platte zusammenhängen. Von besonderem Interesse ist die Tatsache, daß bei einer senkrecht zur Strömung orientierten Platte die kleinsten Koeffizienten in einem zentralen Staugebiet auftreten und die Koeffizienten in Richtung der Ecken zunehmen. Die Strömungsformen werden durch Fotos dargestellt. Es wird gezeigt, daß die Strömung äußerst komplex und dreidimensional ist. Eines der interessanten Ergebnisse ist, daß das Staugebiet von einer zentralen Position bei senkrechter Anströmung weiter nach vorne wandert, wenn die Platte geneigt wird.

ЛОКАЛЬНЫЙ ПЕРЕНОС ТЕПЛА И ГИДРОДИНАМИЧЕСКИЕ ХАРАКТЕРИСТИКИ ПОТОКА ВОЗДУХА, НАПРАВЛЕННОГО ПОД УГЛОМ К КВАДРАТНОЙ ПЛАСТИНЕ

Аннотация — Проведены эксперименты в аэродинамической трубе с целью определения локальных и средних коэффициентов теплообмена и структуры течения жидкости при различных ориентациях квадратной пластины в потоке воздуха. Для определения коэффициентов переноса использовался метод сублимации нафталина, а структура течения вблизи пластины визуализировалась с помощью закопченного стекла. Различные положения пластины при измерениях средних коэффициентов теплообмена расширили диапазон ранее исследованных параметров, и в результате измерений подтвердился вывод о том, что ориентация пластины не влияет на среднее значение коэффициента теплообмена. Локальные значения коэффициентов переноса тепла (или массы) даны на контурных диаграммах, к которых линиями представлены их постоянные значения. Наибольшие значения коэффициентов теплообмена имеют место у краев пластины. Такое положение тесно связано с гидродинамическими явлениями, происходящими у кромки пластины, которые включают не только обычный пограничный слой на передней кромке, но и другие процессы, обязанные конечному размеру пластины. Весьма интересным представляется то, что при ориентации пластины по нормали к потоку коэффициент теплообмена имеет наименьшее значение в зоне торможения в центре пластины и возрастает по мере приближения к краям. Структура течения жидкости представлена на фотографиях, из которых видно, что поток трёхмерный и весьма сложный. Одним из интересных результатов исследования является то, что область торможения смещается от центра, когда поток направлен по нормали к пластине, к краям, когда пластина расположена под углом к потоку.